Copyright © 2015 KSII

Percolation Theory-Based Exposure-Path Prevention for 3D-Wireless Sensor Networks Coverage

Xiaoshuang Liu[1], Guixia Kang[2], Ningbo Zhang[3]
Key Laboratory of Universal Wireless Communication, Ministry of Education,
Beijing University of Posts and Telecommunications
Beijing, PR China
[1] [LXS_55@163.com]
[2] [gxkang@bupt.edu.cn]
[3] [nbzhang@bupt.edu.cn]
*Corresponding author: Ningbo Zhang

Received July 18, 2014; revised October 10, 2014; revised November 25, 2014; accepted November 30, 2014; published January 31, 2015

Abstract

Different from the existing works on coverage problems in wireless sensor networks (WSNs), this paper considers the exposure-path prevention problem by using the percolation theory in three dimensional (3D) WSNs, which can be implemented in intruder detecting applications. In this paper, to avoid the loose bounds of critical density, a bond percolation-based scheme is proposed to put the exposure-path problem into a 3D uniform lattice. Within this scheme, the tighter bonds of critical density for omnidirectional and directional sensor networks under random sensor deployment—a 3D Poisson process are derived. Extensive simulation results show that our scheme generates tighter bounds of critical density with no exposure path in 3D WSNs.

Keywords: 3D wireless sensor networks, exposure-path prevention problem, coverage, percolation theory, critical density.

This work is supported by International Science and Technology Cooperation Project (no. 2010DFA11590), the Important National Science & Technology Specific Projects of the Ministry of Science and Technology of China (no. 2013ZX03006001), New Century Excellent Talents in University (NCET) (no. NCET-11-0593), the National High Technology Research and Development Program of China ("863"Program, No. SQ2015AA010 2085), and National Natural Science Foundation of China (No. NSFC61471064).

http://dx.doi.org/10.3837/tiis.2015.01.008 **ISSN : 1976-7277**

1. Introduction

Wireless sensor networks (WSNs) have a wide area of applications, such as military detection, healthy environment monitoring, and seism surveillance. All of these applications require the intrusions being detected by sensor nodes in the interested region [1]. In the area of WSNs, the intrusion detection problem belongs to node coverage issue, which is of paramount importance. Furthermore, coverage of intrusions path has a great impact on the intrusion detection. Most of the previous researches focus on the full coverage models in WSNs. Full coverage means that everywhere in the deployment area is covered by nodes, which is at the cost of resource wastes and high complexity. In fact, many applications of WSNs mainly concentrate on the exposure-path prevention which needs the partial coverage to prevent the exposure paths. In the other words, they don't need the full coverage, and just need moving detected objects (or intrusions).

Generally, coverage creates collaborations among the nodes in covering a target region for surveying specific phenomena. Firstly, we define a covered region in which each point is covered by at least one sensor node. If an intruder can traverse through the deployment area and the resulting path isn't covered by nodes, we name the traversed path as the exposure path. It reflects the ability of intrusions moving through the deployed area. In [2-3], the authors proposed an approximation algorithm to address the minimum exposure path problem and guarantee the network performance. S. Ferrari and G. Foderaro presented an artificial-potential approach [4] that designed the minimum-exposure paths of multiple mobile objects containing sensor nodes in a dynamic network. In addition, this approach could be used in heterogeneous wireless sensor networks (HWSNs). In allusion to the full coverage, network coverage is rather poor if there exists an exposure path in WSNs. Therefore, we consider the exposure-path prevention problem with the percolation theory in 3D WSNs.

Percolation theory was first put forward by Broadbent and Hammersley to simulate the percolation process of immersed rocks [5], which is appropriate for modeling the disordered media. On the one hand, percolation theory deals with clustering, criticality, diffusion, fractals, phase transitions and disordered systems. It also provides a quantitative model for understanding these phenomena. Therefore, percolation theory is a theoretical and statistical background for various physical and natural sciences. In addition, this theory describes emergent properties related to the connectivity of large numbers of objects. Due to some spatial extent of these objects, their spatial relationships are relevant and statistically prescribed. Thus, percolation theory is related to graph and network theories [6], which exists within the intersection of probability theory and topology. For the present purpose, the chief relevance of percolation theory is its ability to deliver global properties from local properties. In [7], the global properties sought to describe flow, conduction and other transport properties of porous media.

According to percolation theory [8-9], if we assume p as the average degree of connectivity between various sub-units of some arbitrary system, there exists a percolation threshold p_t. When $p \geq p_t$, there is no exposure path from one side of the system to the other. There are some researches that lie in the exposure-path problem and percolation theory, and we will introduce the related works in Section 2.

The existing works [2-7,10] mainly focus on the exposure-path problems in two dimensional (2D) networks. Nevertheless, 3D WSNs are more apt for practice in most

applications [11], and no more contributions are achieved so far. In this paper, we consider the exposure-path prevention problem with percolation theory in 3D WSN scenarios. In order to address this problem and get the tighter bonds of critical density, we put the exposure-path problem into a 3D uniform lattice and propose a bond percolation-based scheme to calculate the tighter bounds of critical density. The scope of the proposed scheme is to detect intrusions in 3D WSNs, which has important practical implications.

The remainder of this paper is organized as follows. Section 2 introduces the related works of barrier coverage and percolation theory. Section 3 presents the system models and problem formulation about exposure-path prevention in 3D WSNs. Section 4 highlights the bond-percolation theory to derive and analyze the optimal critical density for exposure-path problem. Moreover, we discuss the mutual dependence among edges of the proposed bond percolation-based scheme in this section. The models and schemes we proposed is evaluated by the extensive simulation results in Section 5. Section 6 concludes this paper.

2. Related Work

This section introduces the recent results about barrier coverage and percolation theory in WSNs. The exposure-path prevention problem is one part of barrier coverage.

2.1. Barrier Coverage

According to the different covered objects, the researchers classify the coverage of static WSNs into three types: area coverage [12], point coverage [13] and barrier coverage [14], as shown in **Fig. 1(a)-(c)**. The area coverage is full coverage, which requires each point within the target area covered by at least one node,. The point coverage considers the coverage of several discrete targets, i.e., the partial coverage. The barrier coverage focuses on the detection ability of moving targets. In this paper, the mentioned exposure-path problem belongs to the barrier coverage.

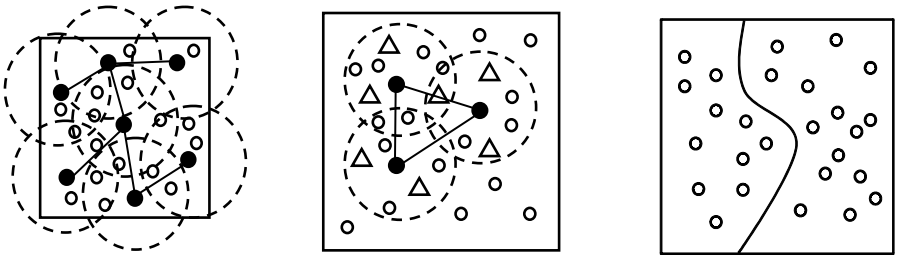

(a) Area coverage (b) Point coverage (c) Barrier coverage

Fig. 1. The coverage problem

The significance of barrier coverage is as follows. For the monitor, it can determine the optimal deployment to make the biggest detection probability. For the intruder, it can choose the most secure path to pass through the monitor area. In [15], Meguerdichian *et al.* firstly introduced the notion and model of barrier coverage in WSNs. They tried to determine the QoS of the optimal or worst coverage, and proposed a centralized algorithm based on Voronoi and Delaunay triangulation partition. The authors of [16] defined a *k-barrier coverage*, and proposed its discriminating algorithms after the deployment. They also presented two probabilistic barrier coverage concepts, namely, *weak* and *strong barrier coverage*. Meanwhile, they derived the minimum number of sensor nodes required to ensure weak barrier coverage with high probability. However, strong barrier coverage is still an open issue.

Most aspects of barrier coverage are researched in some literatures [17-22]. Due to the globalized nature of barrier coverage, it is very difficult to solve the problem in a decentralized way. To address this challenge, Chen *et al.* [17] introduced the concept of local barrier coverage and devised localized sleep-wakeup algorithms to provide near-optimal solutions. In [18], for strong barrier coverage, the authors proposed an efficient distributed algorithm to construct multiple disjoint barriers in a randomly deployed WSN on a long irregular strip region. The algorithm reduced the network delay and communication overhead compared with a centralized solution. In [19], Chen *et al.* studied the quality of barrier coverage and identified where a repair is needed when the barrier performance is less than a predefined value. Saipulla *et al.* [20] investigated the barrier coverage of the line-based deployment rather than the Poisson distribution model. They also derived a tight lower-bound probability of the existence of barrier coverage. G. Yang and D. Qiao [21] exploited the sensing collaboration between sensor nodes to research the weak barrier coverage. The authors of [22] presented an energy efficient scheduling algorithm with a probabilistic sensing model for barrier coverage.

All the above studies are within the scope of omnidirectional and static WSNs. Regarding directional or dynamic WSNs, there are also many studies [23-27]. Wang and Cao [23] introduced a novel full-view coverage model to camera sensor networks. Further, a novel method to select camera sensor nodes from an arbitrary deployment was suggested in [24] to form a camera barrier. Ma *et al.* studied the minimum camera barrier coverage problem in camera sensor networks [25]. In [26], the problem of finding appropriate orientations of directional sensor nodes was investigated to provide strong barrier coverage. With the development of mobile sensors, He *et al.* [27] investigated the cost-effective barrier coverage problem in the circumstances of no sufficient mobile nodes existing, and designed sensor patrolling algorithms to improve barrier coverage.

2.2. Percolation Theory

In [28], Gilbert firstly raised the concept of continuum percolation to find the critical density of a Poisson point process. An unbounded connected component almost surely appears at this density so as to make the network provide long distance multihop communication. For studying continuum percolation, Gilbert's model is the foundation of wireless networks. Percolation threshold is adopted to investigate the connectivity of wireless networks. Penrose [29] indicated that as the number of nodes goes to infinity, the critical range for the probability of establishing overall connectivity is close to 1. This range leads to each node connecting to neighbors on average. Based on the percolation theory, Gupta and Kumar [30] used the correlation results to derive the sufficient condition on communication distance for asymptotic connectivity in wireless networks. However, the loose lower and upper bounds on the critical density restrict the application of continuum-percolation theory.

In [31], for both Poisson and hard-core stationary point processes, the authors demonstrated the existence of site and bond percolation in the Gabriel graph [32]. The simulation results showed that the critical bounds correspond to the existence of two paths of open sites and open bonds, respectively. The authors of [33] presented different classes of coverage algorithms and determined the critical density of a Poisson point process. Simultaneously, they talked about the almost sure existence of an unbounded connected component based on the ratio of the connectivity range of the base stations to the clients'. In [34], Glauche *et al.* discussed a distributed protocol to guarantee strong connectivity in ad hoc networks. Their proposed problem to find the critical communication range of mobile devices could be interpreted as that of determining the critical node neighborhood degree. Above this range, an ad hoc network graph is almost surely connected. The authors of [35] characterized

fundamental coverage properties of large-scale sensor networks in the consideration of both Boolean and probabilistic sensing models for a variety of network scenarios. For efficient topology control of the network, the concept of monotone percolation was put up in [36] based on the local adjustment of the communication radii of the sensor nodes. They also presented some algorithms to guarantee the existence of relatively short paths between any pair of source and destination nodes. Habib *et al.* [37] focused on percolation in coverage and connectivity of 3D WSNs. It was an integrated continuum percolation problem due to the dependency between coverage and connectivity. Therefore, the authors proposed an integrated concentric-sphere model to address coverage and connectivity in an integrated way. Khanjary *et al.* [38] introduced aligned-orientation directional sensor networks, and proposed an approach to calculate the density of nodes at critical percolation in such networks by using continuum percolation. In these networks, sensor nodes were deployed based on a Poisson point process and the orientation of all sensor nodes is the same.

However, most existing percolation-based schemes apply the common continuum-percolation theory, enduring the loose lower and upper bounds on the critical density. Thus, these theoretical results may not be directly applied to most application scenarios of WSNs. To solve this problem, we offer a bond percolation-based scheme through mapping the exposure path-prevention problem into a bond percolation model in 3D WSNs. Depending on the deployment of sensor nodes obeying a 3D Poisson process, we deduce the critical densities for both omnidirectional and directional sensor networks under random sensor deployment.

3. System Models And Problem Formulation

In the beginning, we present the sensing and deployment models of omnidirectional and directional sensor networks. Then, the exposure-path prevention problem is formulated by the continuum-percolation theory [39] in 3D WSNs.

In a vast 3D WSN, we deploy sensor nodes randomly and uniformly whose locations can be modeled as a stationary 3D Poisson distribution with an intensity $\lambda > 0$. In any sub-region V', the number of sensor nodes $N(V') = k$ follows the Poisson distribution with a parameter $\lambda \|V'\|$, where $\|V'\|$ is the volume of V'. Then, the probability intensity function is

$$p(N(V') = k) = \frac{(\lambda \|V'\|)^k}{k!} \exp(-\lambda \|V'\|). \tag{1}$$

3.1. System Models

3.1.1. Omnidirectional sensing Model

We adopt the sphere model (B, r, λ) [11] as the sensing model in omnidirectional sensor networks. In this model, the node sensing range is a spherical region B with sensing radius r, as shown in **Fig. 2(a)**, and λ is the deployment density of the sensor nodes. If $s: (x_s, y_s, z_s)$ denotes a node position in space rectangular coordinate $o-xyz$, a targeted point $t: (x_t, y_t, z_t)$ is said to be covered by s when the Euclidean distance $|st| = \sqrt{(x_s - x_t)^2 + (y_s - y_t)^2 + (z_s - z_t)^2}$ is not larger than r.

(a) Omnidirectional sensing model (b) Directional sensing model

Fig. 2. System models.

3.1.2. Directional sensing Model

Different from the above omnidirectional sensing model, we employ a widely used model — the directional sensing model [40] in the actual applications [41], [42]. As shown in **Fig. 2(b)**, the sensing area is the circular cone $(s,r,\vec{v},\alpha)$, where $\vec{v}$ is the central unit vector termed as sensing direction, and α is the offset angle of the field of view (FOV). t is said to be covered by s if and only if two conditions are satisfied:

1) The Euclidean distance $|st| \le r$;

2) The angle $\overrightarrow{st} \wedge \vec{v}$ between $\overrightarrow{st}$ and $\vec{v}$ is within $[0,\frac{\alpha}{2}]$.

In directional sensor networks, we assume θ is the angle of $\vec{v}$ relative to xoz-plane, and θ is a random variable with the uniform distribution on $[0,2\pi]$, i.e., $\theta \square U[0,2\pi]$.

3.2. Problem Formulation

Let R^3 be the 3D WSN and its volume is V. We partition the deployment space into the covered region C covered by at least one sensor node, and the vacant region W covered by no sensor node. The definition of exposure path in a 3D network is given in the following.

Definition 1: If a continuous strip S (or curve S) belongs to any vacant region W, S from one side to the other side of the deployment region is defined as an exposure path, see **Fig. 3(a)-(b)**.

Sensor nodes may be spread in an arbitrary pattern, as shown in **Fig. 3(a)-(d)**. An exposure path exists in the 3D network if $\lambda \le \lambda_C$ (**Fig. 3(a)-(b)**), and not vice versa (**Fig. 3(c)-(d)**). λ_C is the critical threshold. However, the extortionate density will cause vast redundancy, which leads to high implementation complexity and cost. Therefore, λ is the optimal density when there are no exposure paths and no redundancy in 3D networks.

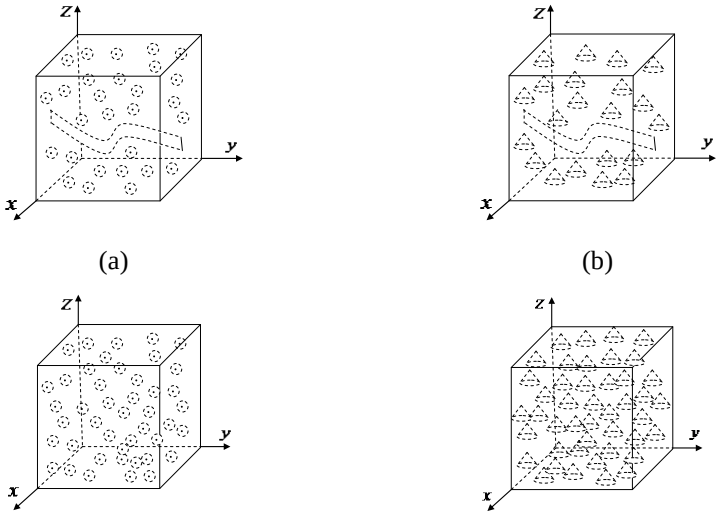

Fig. 3. Relationship between exposure path S and sensor node density λ_C.

Consequently, the exposure-path prevention problem is formulated as the calculation of the critical density λ_C in a 3D network. To get the tighter bounds of λ_C, we apply bond percolation theory for the 3D WSNs in the following sections. On the basis of the theory of limit, strip S can be considered as the countless curves superposition. For simplicity, we just choose one curve of strip S to discuss, denoted as path S.

3.3. Bond percolation model

To solve the exposure-path prevention problem, we divide the 3D sensor network into a 3D uniform lattice. $d(C,\lambda)$ and $d(W,\lambda)$ denote the number of lattices in the regions C and W, respectively. Let the critical density [8] be $\lambda_C = \inf\{\lambda : p(d(C,\lambda)=\infty) > 0\}$. It is simple to derive that there exists an exposure path in the 3D network if $\lambda \le \lambda_C$.

It is assumed that one unit cube region contains n vertexes, i.e., $M = \{m_1, m_2, ..., m_n\}$, forming a $\sqrt[3]{n} \times \sqrt[3]{n} \times \sqrt[3]{n}$ lattice as shown in **Fig. 4**. $\sqrt[3]{n}$ is used to approximately substitute for $\left\lfloor \sqrt[3]{n} \right\rfloor$ for the sake of simplicity, which doesn't affect our final results. The edge between vertex m_i and m_j is denoted as $e_{i,j}$, where $i, j \in [1, n]$. Thus, the edge length of the neighboring vertexes is $\mu = \dfrac{1}{\sqrt[3]{n}}$ (n vertexes don't include the ones which lie on the edges of the cube). The following definitions identify the relationship between $e_{i,j}$ and the lower and upper bounds of λ_C.

Definition 2: For edge $e_{i,j}$, we define

$$L(e_{i,j}) = \begin{cases} 1, \text{if } \textit{at least one} \text{ point on } e_{i,j} \textit{ is} \text{ covered;} \\ 0, \text{if } \textit{all} \text{ points on } e_{i,j} \text{ are } \textit{not} \text{ covered.} \end{cases} \tag{2}$$

Then, if $L(e_{i,j})=1$, $e_{i,j}$ is defined as L-closed edge; if $L(e_{i,j})=0$, $e_{i,j}$ is called as L-open edge.

$$U(e_{i,j})=\begin{cases}1, & \text{if } all \text{ points on } e_{i,j} \text{ are covered;}\\ 0, & \text{if } at\ least\ one \text{ point on } e_{i,j} \text{ is } not \text{ covered.}\end{cases} \tag{3}$$

Thus, if $U(e_{i,j})=1$, $e_{i,j}$ is named as U-closed edge; if $U(e_{i,j})=0$, $e_{i,j}$ is denoted as U-open edge.

Definition 3: Let Z^3 be the 3D lattice with vertex set M, edge set E and $|M|=n$. If $e_{i,j}$ between arbitrary two neighboring is L-closed/L-open, Z^3 is said to be an L-coverage lattice; If it is U-closed or U-open, Z^3 is called a U-coverage lattice.

Definition 4: A path S in Z^3 goes via a sequence of edges $e_{1,2},e_{2,3},...,e_{i,i+1},...$, $i\geq 1$, if all the edges in S are L-open/U-open, S is named the L-open/U-open path; if all the edges are L-closed/U-closed, S is called the L-closed/U-closed path.

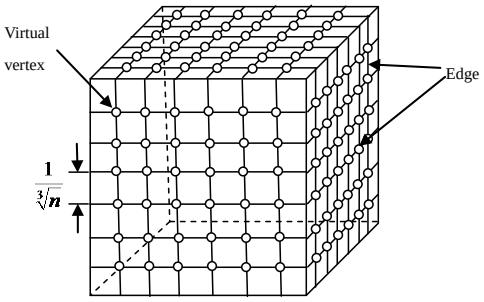

Fig. 4. The unit cube region with a virtual lattice.

With the above definitions, we derive that: 1) if edge $e_{i,j}$ is the U-closed edge, then it must be the L-closed edge in terms of coverage; 2) the upper bound λ_u of the critical density λ_C could be derived by U-coverage lattice, and the lower bound λ_l by L-coverage lattice for 3D sensor networks.

4. Bounds of Critical Density

In this paper, if p is the probability of an arbitrary edge being closed in the 3D lattice, a threshold value $p_t\in[0,1]$ exists and results in the differences of the global behavior of the system in two regions C and W. Generally, for all $p>p_t$, there exists one closed path from one side to the other of the 3D network. On the contrary, there is no closed path for all $p<p_t$. To ease presentation, we define $P_L=p\{\mathrm{L}(e_{i,j})=1\}$, $P_U=p\{U(e_{i,j})=1\}$; and $\lambda_l=\sup\{\lambda:P_L\leq p_t\}$, $\lambda_u=\inf\{\lambda:P_U\geq p_t\}$. Then, we have $p\{\text{the exposure path exists}\}>0$ if $P_L<p_t$, and $p\{\text{the exposure path exists }\}=0$ if $P_U>p_t$.

4.1. Critical Density λ_C

4.1.1. λ_C of Omnidirectional Sensor Nodes

As shown in **Fig. 5(a)**, s_n is one arbitrary point on edge $e_{i,j}$ of the L-coverage lattice, and we define an operator '$\cup$': $A_i \cup A_j \triangleq \bigcup_{\forall s_n \in e_{i,j}} A_n$ in this paper, where A_n is the sphere centered at s_n with radius r. Then, $A_i \cup A_j$ is a set containing all the coverage spheres centered at the points of $e_{i,j}$.

Lemma 1: No sensor node in $A_i \cup A_j$ is a sufficient and necessary condition of all points on $e_{i,j}$ being not covered.

Proof: Based on the definition of $A_i \cup A_j$, it contains the total coverage space of all points on $e_{i,j}$. Therefore, it is clear that if there is no sensor nodes in $A_i \cup A_j$, all points on $e_{i,j}$ aren't covered by any sensor nodes. The reverse is also true.

Next, we exploit $e_{i,j}$ on y-axis as an example and draw the following conclusion. m_i and m_j are the two endpoints of edge $e_{i,j}$.

Theorem 1: In 3D omnidirectional sensor networks, we have

$$\lambda_l = \frac{-\ln(1-p_t)}{\frac{4}{3}\pi r^3 + \frac{\pi r^2}{\sqrt[3]{n}}} < \lambda_C < \lambda_u = \frac{-\ln(1-p_t)}{\frac{2\pi}{3}(2r+\frac{1}{2\sqrt[3]{n}})(r-\frac{1}{2\sqrt[3]{n}})^2}. \tag{4}$$

Proof: Following are three steps to prove the theorem.

1) From (1), we have $p\{N(A_i \cup A_j)=0\} = \exp(-\lambda \|A_i \cup A_j\|) = \exp(-\lambda(\frac{4}{3}\pi r^3 + \frac{\pi r^2}{\sqrt[3]{n}}))$.

Then, $P_L = 1 - p\{L(e_{i,j})=0\} = 1 - \exp(-\lambda(\frac{4}{3}\pi r^3 + \frac{\pi r^2}{\sqrt[3]{n}}))$.

Consequently, P_L increases monotonously as λ increases. Since $\lambda_l = \sup\{\lambda : P_L \le p_t\}$, $1-\exp(-\lambda_l(\frac{4}{3}\pi r^3 + \frac{\pi r^2}{\sqrt[3]{n}})) = p_t$. Therefore, we can get λ_l in (4).

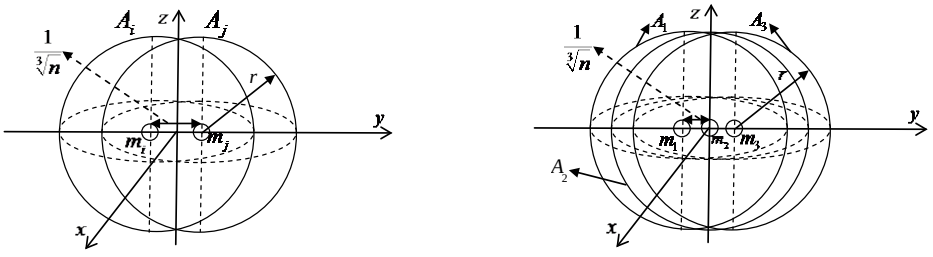

Fig. 5. Covered region division of the edge $e_{i,j}$.

2) Based on the above analysis, the probability of all points on $e_{i,j}$ being covered is difficult to derive the explicit expression. As a result, we need to find an approximation of P_U. We denote P_o as the probability that all points on $e_{i,j}$ are covered by one sensor node. Since P_U is the probability that all points on $e_{i,j}$ are covered by one sensor network, obviously,

$$P_U > P\{\text{all points on } e_{i,j} \text{ are covered by one sensor node}\} = P_o .$$

It is clear that one sensor node covers all points on $e_{i,j}$ if and only if some sensor node exists in $A_i \bigcap A_j$. From (1),

$$p\{N(A_i \bigcap A_j) > 0\} = 1 - \exp(-\lambda \left\| A_i \bigcap A_j \right\|) . \tag{5}$$

Let $A = \left\| A_i \bigcap A_j \right\|$. According to **Fig. 5(a)**, we can obtain

$$P_U > 1 - \exp(-\lambda \iint_R 4\sqrt{r^2 - (x')^2 - (y' - \frac{1}{2\sqrt[3]{n}})^2}\, d\sigma)) , \tag{6}$$

where an arbitrary point in $A_i \bigcap A_j$ is (x', y', z'), $R: (x')^2 + (y')^2 = (r - \frac{1}{2\sqrt[3]{n}})^2$, and $d\sigma = dx'dy'$. It is easy to obtain $A = \frac{2\pi}{3}(2r + \frac{1}{2\sqrt[3]{n}})(r - \frac{1}{2\sqrt[3]{n}})^2$.

As a consequence, we choose P_o as the approximation of P_U. Let $\lambda_u = \inf\{\lambda : P_o \geq p_t\}$. Then we can get λ_u in (4).

3) Equation (3) is equal to

$$U(e_{i,j}) = \begin{cases} 1, \text{if } e_{i,j} \text{ is covered by one sensor node;} \\ 0, \text{otherwise.} \end{cases} . \tag{7}$$

If $P_L < p_t$, then $p\{d(W) = \infty)\} > 0$. It is easy to know that $\lambda_l < \lambda'_C$. From (6), if $1 - \exp(-\lambda A) > p_t$, then $P_U > p_t$. In consequence, we can derive that if $1 - \exp(-\lambda A) > p_t$, then $p\{d(C) = \infty)\} > 0$. According to the definition of λ_C, we have $\frac{-\ln(1 - p_t)}{A} > \lambda_C$. From 1) and 2), we gain the **Theorem 1**.

4.1.2. λ_C of Directional Sensor Nodes

In **Fig. 6,** we assume a directional sensor node locates an arbitrary point $F(x_f, y_f, z_f)$ in $A_i \cup A_j$. The sphere centered at F with radius r intersects y -axis at

$F_1(0, y_f - \sqrt{r^2 - x_f^2 - z_f^2}, 0)$ and $F_2(0, y_f + \sqrt{r^2 - x_f^2 - z_f^2}, 0)$, using $e_{i,j}$ on y-axis as an example in **Fig. 6(a)-(d)**. For simplicity, let $f_1 = y_f - \sqrt{r^2 - x_f^2 - z_f^2}$, $f_2 = y_f + \sqrt{r^2 - x_f^2 - z_f^2}$, and $\vec{\gamma} \wedge \vec{\eta}$ be the angle between vector $\vec{\gamma}$ and $\vec{\eta}$. Based on the theory of limit, the circular cone ψ is known as the countless sectors superposition. Firstly, one sector ϖ is considered in ψ. Then, through the countless sectors superposition, we have **Theorem 2**.

Theorem 2: In 3D directional sensor networks, we have

$$\lambda_l = \frac{-\ln(1-p_t)}{\int_{A_i \cup A_j} (1 - P_N) d\nu} < \lambda_C < \lambda_u = \frac{-\ln(1-p_t)}{\int_{A_i \bigcap A_j} (1 - P'_N) d\nu}, \tag{8}$$

where $d\nu = dxdydz$,

$$P_N = \begin{cases} \dfrac{2\pi - \alpha - \overrightarrow{FF_1} \wedge \overrightarrow{Fm_j}}{2\pi}, if -\dfrac{1}{2\sqrt[3]{n}} < f_1 < \dfrac{1}{2\sqrt[3]{n}} and\ f_2 > \dfrac{1}{2\sqrt[3]{n}}; \\ \dfrac{2\pi - \alpha - \overrightarrow{Fm_i} \wedge \overrightarrow{Fm_j}}{2\pi}, if\ f_1 < -\dfrac{1}{2\sqrt[3]{n}} and\ f_2 > \dfrac{1}{2\sqrt[3]{n}}; \\ \dfrac{2\pi - \alpha - \overrightarrow{FF_1} \wedge \overrightarrow{FF_2}}{2\pi}, if -\dfrac{1}{2\sqrt[3]{n}} < f_1 < f_2 < \dfrac{1}{2\sqrt[3]{n}}; \\ \dfrac{2\pi - \alpha - \overrightarrow{Fm_i} \wedge \overrightarrow{FF_2}}{2\pi}, if\ f_1 < -\dfrac{1}{2\sqrt[3]{n}} and -\dfrac{1}{2\sqrt[3]{n}} < f_2 < \dfrac{1}{2\sqrt[3]{n}}. \end{cases}$$ and

$$P'_N = \begin{cases} 1, & if\ \overrightarrow{Fm_i} \wedge \overrightarrow{Fm_j} < \alpha; \\ \dfrac{2\pi - \alpha + \overrightarrow{Fm_i} \wedge \overrightarrow{Fm_j}}{2\pi}, & otherwise. \end{cases}.$$

Proof: Three steps are needed to verify this theorem.

1) We assume the probability P_N that all points on edge $e_{i,j}$ are not covered by a directional sensor node $(F, r, \vec{v}, \alpha)$. m_i and m_j are the two endpoints of edge $e_{i,j}$. According to the different positions of F_1, F_2 relative to m_i and m_j, the following conditions are obtained in **Fig. 6(a)-(d)**. θ is depicted in this figure. In order to simplify drawing, we just describe θ in one side of the vertical dashed line.

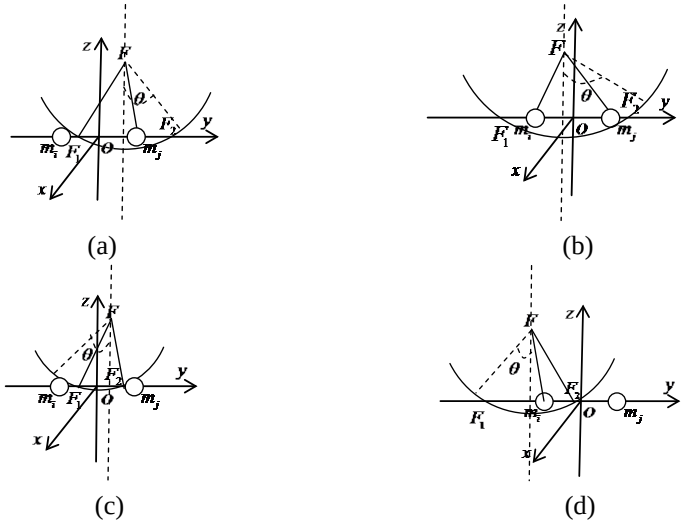

Fig. 6. The relative positions of F_1, F_2, m_i and m_j.

1. If $-\frac{1}{2\sqrt[3]{n}} < f_1 < \frac{1}{2\sqrt[3]{n}}$ and $f_2 > \frac{1}{2\sqrt[3]{n}}$ in **Fig. 6(a)**, the node can't cover any point on $e_{i,j}$ if and only if the angle θ is smaller than the angle of $\overrightarrow{FF_1}$ minus $\frac{\alpha}{2}$, and is larger than the angle of $\overrightarrow{Fm_j}$ plus $\frac{\alpha}{2}$. $\theta \in [0, 2\pi]$. Therefore,

$$P_N = \frac{2\pi - \alpha - \overrightarrow{FF_1} \wedge \overrightarrow{Fm_j}}{2\pi}. \tag{9}$$

Analogously, we have the following conclusions.

2. In **Fig. 6(b)**, if $f_1 < -\frac{1}{2\sqrt[2]{n}}$ and $f_2 > \frac{1}{2\sqrt[3]{n}}$, thus,

$$P_N = \frac{2\pi - \alpha - \overrightarrow{Fm_i} \wedge \overrightarrow{Fm_j}}{2\pi}. \tag{10}$$

3. In **Fig. 6(c)**, if $-\frac{1}{2\sqrt[3]{n}} < f_1 < f_2 < \frac{1}{2\sqrt[3]{n}}$, then,

$$P_N = \frac{2\pi - \alpha - \overrightarrow{FF_1} \wedge \overrightarrow{FF_2}}{2\pi}. \tag{11}$$

4. In **Fig. 6(d)**, if $f_1 < -\frac{1}{2\sqrt[2]{n}}$ and $-\frac{1}{2\sqrt[3]{n}} < f_2 < \frac{1}{2\sqrt[3]{n}}$, hence,

$$P_N = \frac{2\pi - \alpha - \overrightarrow{Fm_i} \wedge \overrightarrow{FF_2}}{2\pi}. \tag{12}$$

With the calculus theory, the region $A_i \cup A_j$ is divided into u small enough regions, R_1, R_2, …, R_u. The circular cone ψ is divided into g small sectors, ϖ_1, ϖ_2, …, ϖ_g. When $u \to \infty$ and $g \to \infty$, the differential $dv = dxdydz$ of volume equal to $\|R_q\|$, $1 \le q \le u$. Let P_q be the probability that no sensor node cover $e_{i,j}$ in R_q. Then, from (1) we have

$$p\{L(e_{i,j}) = 0\} = \prod_{h=1}^{g}\prod_{q=1}^{u} P_q = \prod_{h=1}^{g}\prod_{q=1}^{u} e^{-\lambda dv(1-P_N)} = e^{-\lambda \sum_{h=1}^{g}\sum_{q=1}^{u}(1-P_N)dv}. \tag{13}$$

As $u \to \infty$ and $g \to \infty$,

$$P_L = 1 - e^{-\lambda \int_{A_i \cup A_j}(1-P_N)dv}. \tag{14}$$

Based on (9)-(12), P_L increases monotonously with the increase of λ. So, based on the Section 4, we solve $1 - e^{-\lambda_l \int_{A_i \cup A_j}(1-P_N)dv} = p_t$ to get λ_l.

2) **Fig. 5** indicates that all points on $e_{i,j}$ are covered by one sensor node, if and only if the two conditions are satisfied: a. the sensor node locates in $A_i \bigcap A_j$; b. $\vec{v} \wedge \overrightarrow{Fm_i} < \frac{\alpha}{2}$, $\vec{v} \wedge \overrightarrow{Fm_j} < \frac{\alpha}{2}$. P_o denotes the probability that all points on $e_{i,j}$ are covered by one sensor node. We consider the probability P'_N that the directional sensor node in $A_i \bigcap A_j$ can't cover all points on $e_{i,j}$. It is easy to see that $P'_N = 1$ when $\overrightarrow{Fm_i} \wedge \overrightarrow{Fm_j} < \alpha$, if not, $P'_N = \frac{2\pi - \alpha + \overrightarrow{Fm_i} \wedge \overrightarrow{Fm_j}}{2\pi}$. Similar to 1), we divide the region $A_i \bigcap A_j$ into u small enough regions whose volume is roughly equal to dv. From (13)-(14), we have

$$P_o = 1 - P'_N = 1 - e^{-\lambda \int_{A_i \cap A_j}(1-P'_N)dv}, u \to \infty \; and \; g \to \infty. \tag{15}$$

Therefore, we obtain λ_u in (8).

3) From Section 4.1.2, 1) and 2), we achieve **Theorem 2**.

4.2. Dependence Among Neighboring Edges

From (4) and (8), different values of μ, r and P_N can generate the different bounds. It is obvious that the probabilities of all edges $e_{i,j}$ being open or closed are independent in the bond percolation [2]. However, in this paper, P_L (P_U) of a given edge is dependent on the neighboring edges, but independent on most edges. Consequently, the bond percolation model is used to approximate the coverage percolation.

In this section, the quantitative measure of dependence between $e_{1,2}$ and $e_{2,3}$ is illustrated as an example. We use mutual information in Information Theroy to measure the mutual dependence between $B = L(e_{1,2})$ and $C = L(e_{2,3})$, i.e.,

$$I(B,C) = \sum_{b\in\{0,1\}} \sum_{c\in\{0,1\}} P_{BC}(b,c) \log\left(\frac{P_{BC}(b,c)}{P_B(b)P_C(c)}\right), \tag{16}$$

where $P_{BC}(b,c) = p\{L(e_{1,2}) = b, L(e_{2,3}) = c\}$, $P_B(b) = p\{L(e_{1,2}) = b\}$ and $P_C(c) = p\{L(e_{2,3}) = c\}$. Next, we discuss the mutual dependence in omnidirectional sensor networks.

In **Fig. 5(b)**, $I(B,C)$ reveals the relationships based on μ, r and the dependence. From (1), we have

$$P_B(0) = P_C(0) = \exp\left(-\lambda_l\left(\frac{4}{3}\pi r^3 + \pi r^2 \mu\right)\right),$$

$$P_B(1) = P_C(1) = 1 - \exp\left(-\lambda_l\left(\frac{4}{3}\pi r^3 + \pi r^2 \mu\right)\right).$$

Moreover,

$$P_{BC}(0,0) = p\{N(A_i \cup A_j) = 0\} = e^{-\lambda_l\left(\frac{4}{3}\pi r^3 + 2\pi r^2 \mu\right)},$$

$$P_{BC}(1,0) = P_{BC}(0,1) = P_B(0) - P_{BC}(0,0) = e^{-\lambda_l\left(\frac{4}{3}\pi r^3 + \pi r^2 \mu\right)} - e^{-\lambda_l\left(\frac{4}{3}\pi r^3 + 2\pi r^2 \mu\right)},$$

$$P_{BC}(1,1) = 1 - P_{BC}(0,1) - P_{BC}(1,0) - P_{BC}(0,0) = 1 + e^{-\lambda_l\left(\frac{4}{3}\pi r^3 + 2\pi r^2 \mu\right)} - 2e^{-\lambda_l\left(\frac{4}{3}\pi r^3 + \pi r^2 \mu\right)}.$$

Put these above equations into (16), we get $I(L(e_{1,2}), L(e_{2,3}))$. Given that the case of $I(U(e_{1,2}), U(e_{2,3}))$ is similar to the above, and similar conclusions can also be calculated. When $r = 4$, $\mu = 1$ or 2, we plot the curves of $I(L(e_{1,2}), L(e_{2,3}))$ and $I(U(e_{1,2}), U(e_{2,3}))$ in **Fig.7**. Through the observation, we find that the dependence between neighboring edges is weak. Therefore, the bond percolation model can be used to approximate the coverage percolation.

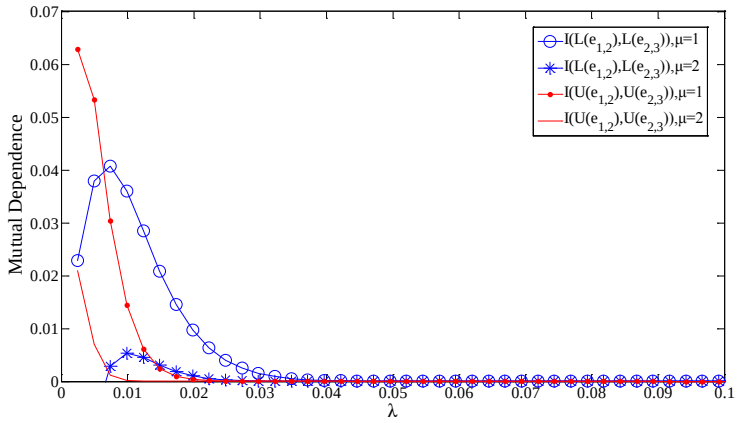

Fig. 7. Comparison between $I(L(e_{1,2}),L(e_{2,3}))$ and $I(U(e_{1,2}),U(e_{2,3}))$ with different μ.

Similarly, after similar calculations and drawing with Matlab, mutual information $I(B,C)$ for directional sensor networks can also be derived, as shown in **Fig. 8**. When $\alpha=\frac{2}{3}\pi$, $I(L(e_{1,2}),L(e_{2,3}))$ and $I(U(e_{1,2}),U(e_{2,3}))$ are close to 0. For random θ, it is easy to see that any two neighboring edges in directional sensor networks are nearly independent with each other, here no longer expatiatory. To sum up, the coverage percolation can be approximately regarded as a bond percolation model.

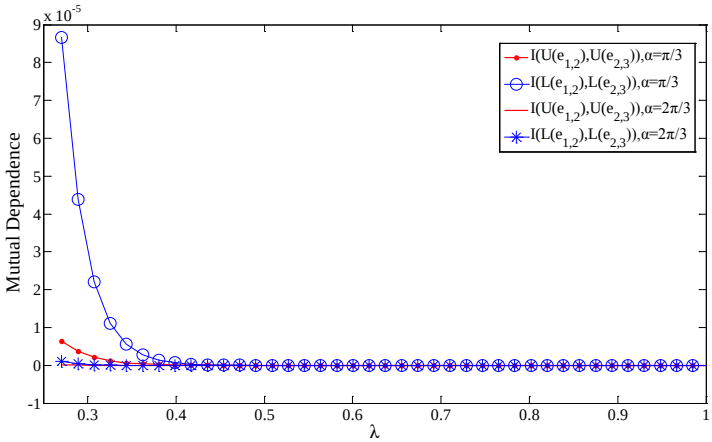

Fig. 8. Comparison between $I(L(e_{1,2}),L(e_{2,3}))$ and $I(U(e_{1,2}),U(e_{2,3}))$ with different α.

5. Simulation Evaluations

Finally, the effectiveness of our model and theoretical analyses are demonstrated through simulation with Matlab 7.0 in this section. Here, sensor nodes are deployed under the stationary 3D Poisson point process. The deployment region is a $100\times100\times100\text{m}^3$ cube. With the simulation results, we analyze the experimental critical densities in L-coverage lattice and U-coverage lattice, respectively.

5.1. Omnidirectional Sensor Networks

Let $r=10$ and p_t=0.5. The number of sensor nodes N_V varies from 100 to 1000 per 20 steps. Then, the density λ varies from 0.0001 to 0.001 per 0.00002 steps. For every λ, 50 different (B, r, λ) are randomly generated. The probability of no exposure path existing is denoted by P_N. Three different P_N corresponding to the continuum percolation, the L-coverage lattice, and the U-coverage lattice, $P_{N,C}$, $P_{N,L}$ and $P_{N,U}$, are obtained for each (B, r, λ), respectively.

Fig. 9 shows the relationship between λ and the probability $P_c = p\{e_{i,j}\ is\ closed\}$. As λ increases, P_c increases. According to **Definition 2-4**, we get the theoretical values P_L and P_o which are close to the simulation values P_L' and P_o', respectively. Clearly, P_L and P_L' are larger than P_o and P_o'. Furthermore, we get the value of P_U' by simulation which is slightly larger than P_o' and less than P_L'.

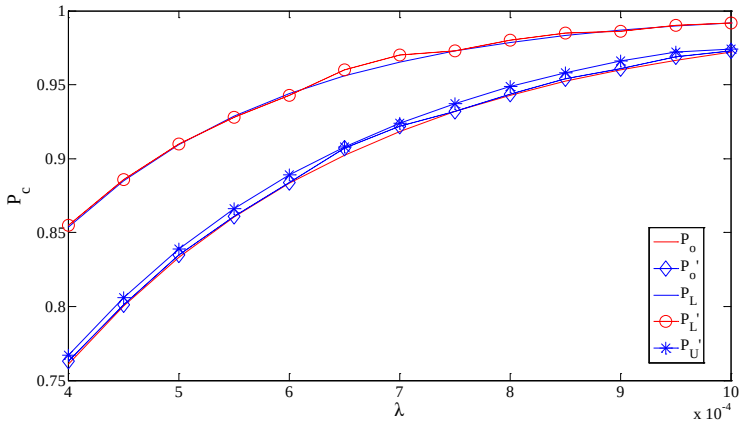

Fig. 9. Relationship between λ and P_c.

Substituting $r=10$ and $\mu=2$ into (4), we obtain $0.00014421<\lambda_C<0.0001936$. The simulation results are $\lambda_l'=0.000137$, $\lambda_u'=0.000189$ and $\lambda_C'=0.000176$. As shown in **Fig. 10(a)**, $P_{N,C}$, $P_{N,L}$ and $P_{N,U}$ increase with the increase of λ, and the simulation result of λ_C is consistent with the theoretical analysis in **Theorem 1**.

Analogously, we do the experiments with different r and μ. Then, the corresponding curves of $P_{N,C}$, $P_{N,L}$ and $P_{N,U}$ are obtained in **Fig. 10(b)-(c)**. $P_{N,C}$, $P_{N,L}$ and $P_{N,U}$ also increase with the increase of λ. When $r=10$ and $\mu=4$, we get $0.00012754<\lambda_C<0.00023388$ from (4). The simulation results are $\lambda_l'=0.000121$, $\lambda_u'=0.000227$ and $\lambda_C'=0.000199$, which are consistent with the analytical results in **Theorem 1**, as shown in **Fig. 10(b)**.

In **Fig. 10(c)**, $P_{N,C}$, $P_{N,L}$ and $P_{N,U}$ also increase with the increase of λ. When $r=11$ and $\mu=2$, we obtain $0.00010965<\lambda_c<0.00014318$ according to (4). The simulation results $\lambda_l'=0.000101$, $\lambda_u'=0.000137$ and $\lambda_C'=0.000128$, which are consistent with the analytical results in **Theorem 1**.

These results of many experiments imply that:

1) The bonds of λ_C becomes looser as μ increases.

2) The bonds of λ_C gets tighter as r increases.

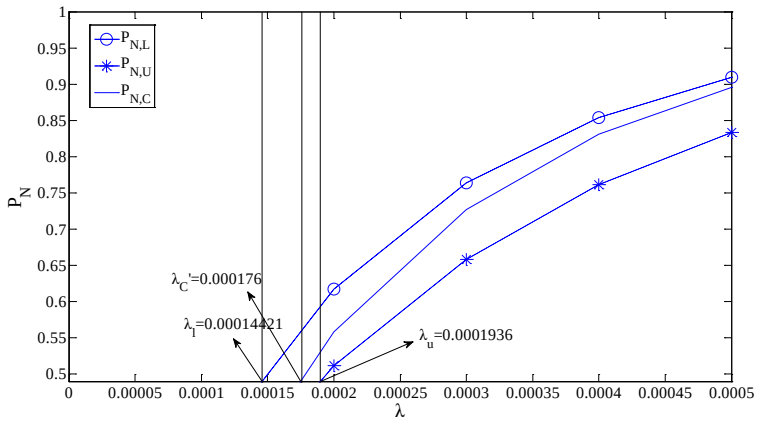

(a) $r = 10$ and $\mu = 2$

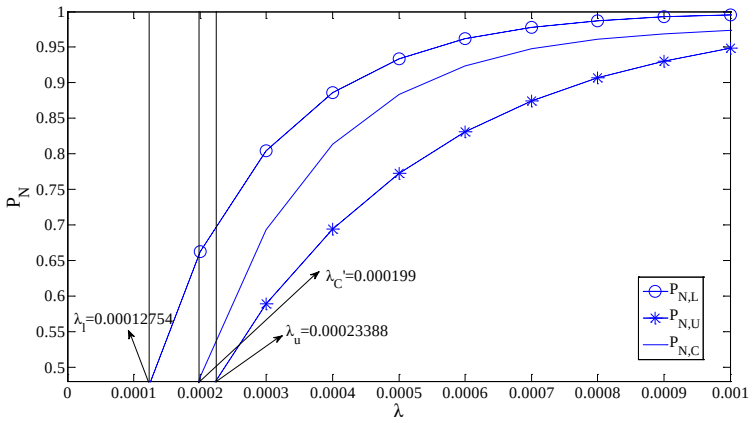

(b) $r = 10$ and $\mu = 4$

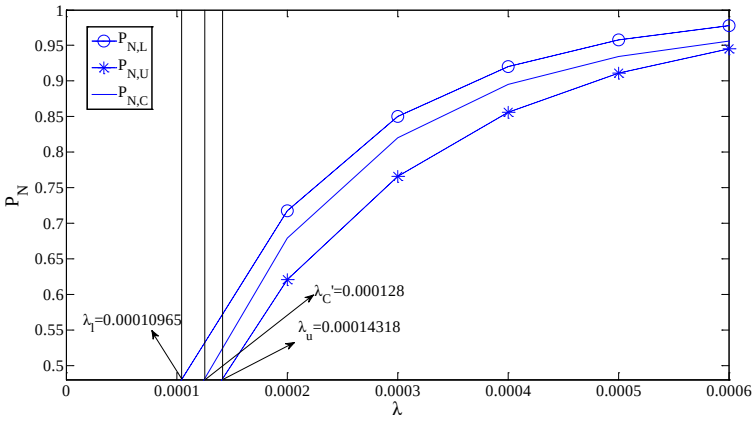

(c) $r = 11$ and $\mu = 2$

Fig. 10. Relationship between P_N and λ with different r and μ.

For the convenience, we first put the scheme [11] denoted as CDMN (Critical Density of Wireless Multi-Hop Networks) into our proposed 3D omnidirectional network model. Then, we define our proposed scheme as PTEP (Percolation Theory-Based Exposure-Path Prevention). **Fig. 11** shows the comparison of critical density between CDMN and PTEP when $r=10$ and $\mu=2$. λ_L and λ_U are the lower and upper bounds of PTEP, while λ'_L and λ'_U are the lower and upper bounds of CDMN, respectively. The corresponding curves $P_{N,L}$, $P_{N,U}$, and $P'_{N,L}$, $P'_{N,U}$ are obtained from CDMN and PTEP, respectively. From this figure, $\lambda'_L = 0.1\times10^{-3}$, $\lambda_L = 0.14421\times10^{-3}$, $\lambda_U = 0.1936\times10^{-3}$, and $\lambda'_U = 0.3\times10^{-3}$. It can be concluded that the bounds of critical density given by CDMN are very loose such that they can not be applied to determine a practically useful density for sensor nodes deployment process. The lower and upper bounds of PTEP are tighter than CDMN's, and we could implement PTEP in 3D WSNs coverage to prevent exposure paths.

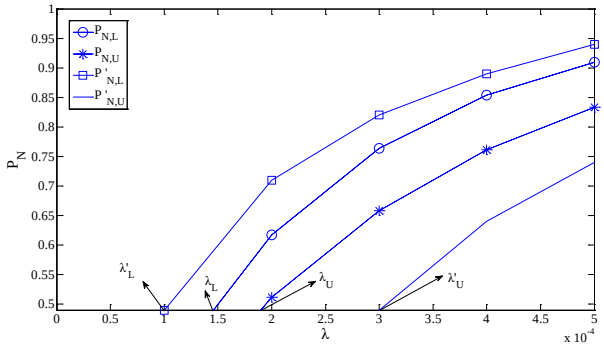

Fig. 11. Comparision of λ between PTEP and CDMN with r=10 and μ=2.

5.2. Directional Sensor Networks

Let $r=10$ and $\alpha=\frac{\pi}{3}$. In the same way, we set that the number of sensor nodes N_V varies from 500 to 2500 per 50 steps. Thus, the density λ varies from 0.0005 to 0.0025 per 0.00005 steps. For each different value of λ, we generate 50 different $(s,r,\vec{v},\alpha)$ randomly generated.

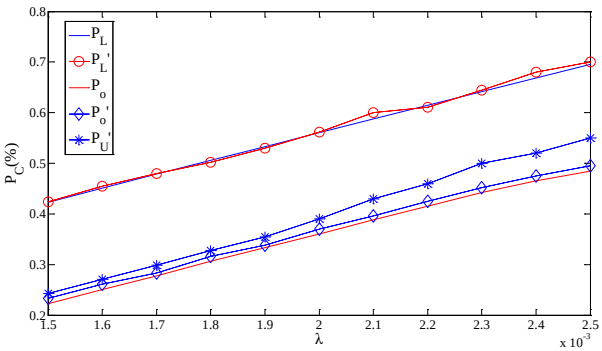

Fig. 12. Relationship between λ and P_c.

In **Fig. 12**, it shows the relationship between λ and $P_c = p\{e_{i,j}\ is\ closed\}$. P_c increases as λ increases. According to (14)-(15) and simulation results, we get the analytical values P_L,

P_o and the simulation values P_L', P_o'. From **Fig. 12**, P_L basically is equal to P_L', and P_o is less than P_o' by 1%. Obviously, P_L and P_L' are larger than P_o and P_o', approximately 0.18. Moreover, the value of P_U' is obtained by simulation which is slightly bigger than P_o'.

We substitute $r=10$ and $\alpha=\frac{\pi}{3}$ into (8), and obtain $0.000712<\lambda_C<0.00210$. The simulation results are $\lambda_l'=0.000720$, $\lambda_u'=0.00202$ and $\lambda_C'=0.00190$. As shown in **Fig. 13(a)**, $P_{N,C}$, $P_{N,L}$ and $P_{N,U}$ also increase as the increase of λ. Then, we conclude that the simulation result of λ_C is consistent with the analytical results in **Theorem 2**.

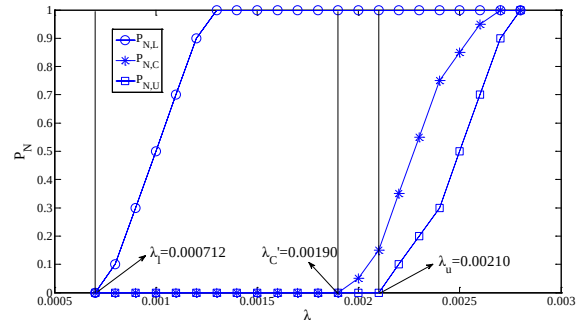

(a) $r=10$ and $\alpha=\frac{\pi}{3}$

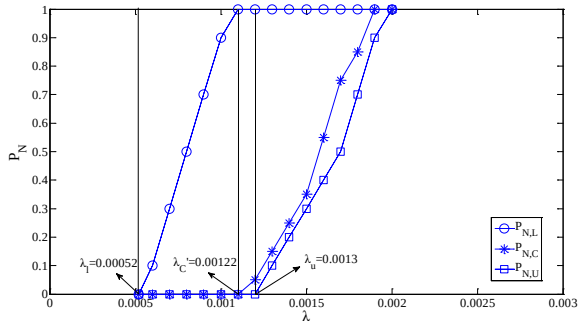

(b) $r=10$ and $\alpha=\frac{2\pi}{3}$

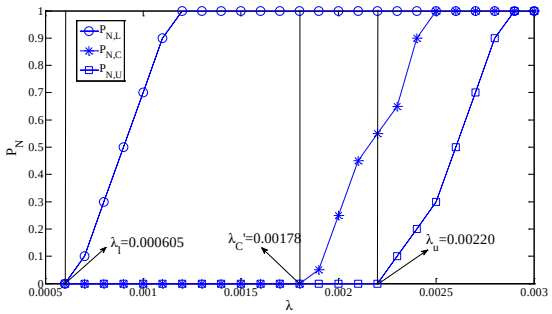

(c) $r=15$ and $\alpha=\frac{\pi}{3}$

Fig. 13. Relationship between P_N and λ with different α.

Similarly, we do the experiments with different r and α. **Fig. 13(b)-(c)** show the relationship between P_N and λ. In the three figures, $P_{N,C}$, $P_{N,L}$ and $P_{N,U}$ also increase as λ increases. When $r=10$ and $\alpha=\frac{2\pi}{3}$, we get $0.00052<\lambda_C<0.0013$ from (8) as shown in **Fig. 13(b)**. The simulation results are $\lambda_l'=0.00051$, $\lambda_u'=0.00128$ and $\lambda_C'=0.00122$, which are consistent with the analytical results in **Theorem 2**.

In **Fig. 13(c)**, when $r=15$ and $\alpha=\frac{\pi}{3}$, we do the calculation from (8), and get $0.000605<\lambda_C<0.00220$. The simulation results $\lambda_l'=0.000684$, $\lambda_u'=0.00223$ and $\lambda_C'=0.00178$ are consistent with the analytical results in **Theorem 2**.

All of the above results imply that:

1) The bonds of λ_C becomes tighter as the increase of α.

2) The bonds of λ_C gets looser as r increases.

To facilitate discussion, we also put CDMN [11] into our proposed 3D directional network model. When $r=10$ and $\alpha=\frac{\pi}{3}$, **Fig. 14** demonstrates the comparison of the lower and upper bounds between CDMN and PEPT. Let λ_L, λ_U and λ'_L, λ'_U be the lower and upper bounds of PTEP and CDMN, respectively. In **Fig. 14,** $\lambda'_L=0.712\times10^{-3}$, $\lambda_L=0.712\times10^{-3}$, $\lambda_U=2.1\times10^{-3}$, $\lambda'_U=2.5\times10^{-3}$. And the corresponding curves $P_{N,L}$, $P_{N,U}$, and $P'_{N,L}$, $P'_{N,U}$ are obtained from PTEP and CDMN, respectively. The simulation results show that the lower bound of CDMN is close to the lower bound of PTEP, while its upper bound is larger than PTEP's. Hence, the bounds of critical density given by CDMN are very loose. So we can not apply them to determine a practically useful density for 3D-network deployment. Conversely, due to the tighter lower and upper bounds of PTEP, it could be implemented to address the exposure-path prevention problem in 3D WSNs.

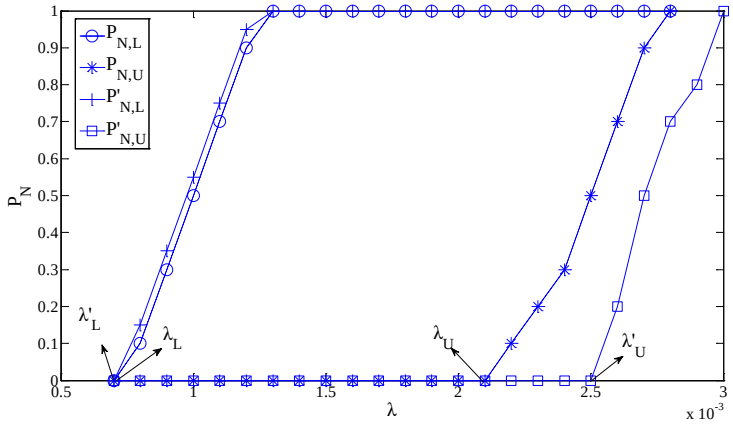

Fig. 14. Comparision of λ between PTEP and CDMN with r=10 and $\alpha=\frac{\pi}{3}$.

6. Conclusion

In this paper, the exposure-path prevention problem with the percolation theory was considered in 3D omnidirectional and directional WSNs, which could be applied in intruder detecting applications. In order to solve this problem, we put it into a 3D uniform lattice and proposed a bond percolation-based scheme to calculate the tighter bounds of critical density. The proposed models and simulation results demonstrated that our scheme generated tighter bounds of critical density and ruled out the exposure path in 3D WSNs. To prevent exposure paths in 3D WSNs is still our future research field.

References

[1] L. Atzori, A. Iera, and G. Morabito, "The Internet of Things: A survey," *Comput. Netw.*, vol. 54, no. 15, pp. 2787–2805, 2010. Article (CrossRef Link)
[2] H. Djidjev, "Efficient computation of minimum exposure paths in a sensor network field," in *Proc. of DCOSS*, vol. LNCS 4549. Feb. 2007, pp. 295–308. Article (CrossRef Link)
[3] H. Djidjev, "Approximation algorithms for computing minimum exposure paths in a sensor field," *ACM Trans. Sensor Netw.*, vol. 7, no. 3, pp. 1–3, Sep. 2010. Article (CrossRef Link)
[4] S. Ferrari and G. Foderaro, "A Potential field approach to finding minimum-exposure paths in wireless sensor networks," in *Proc. of IEEE Int. Conf. Robot. Autom. Anchorage Conv. District*, May 2010, pp. 335–341. Article (CrossRef Link)
[5] Broadbent S R, Hammersley J M, "Percolation processes I. Crystals and mazes," *Proceedings of the Cambridge Philosophical Society (S0305-0041)*, 1957, 53(4): 629-641. Article (CrossRef Link)
[6] Stauffer, Dietrich, Aharony, Amnon, "Introduction to percolation theory," *London: Taylor and Francis (519.237.8)*, 1991, pp: 2-5. Article (CrossRef Link)
[7] A Hunt, R Ewing, B Ghanbarian, "Percolation Theory for Flow in Porous Media Lecture Notes in Physics," Volume 880, 2014, pp: 1-35. Article (CrossRef Link)
[8] Aharony A, Stauffer D, "Introduction to percolation theory," *Taylor & Francis*, 2003. Article (CrossRef Link)
[9] G. Grimmett, "What is Percolation?" 2nd ed. New York, NY, USA: Springer-Verlag, 1999. Article (CrossRef Link)
[10] Liang Liu; Xi Zhang; Huadong Ma, "Percolation Theory-Based Exposure-Path Prevention for Wireless Sensor Networks Coverage in Internet of Things," *Sensors Journal, IEEE* , vol.13, no.10, pp.3625,3636, Oct. 2013. Article (CrossRef Link)
[11] Ng S C, Mao G, Anderson B D O, "Critical density for connectivity in 2D and 3D wireless multi-hop networks," *Wireless Communications, IEEE Transactions on*, 2013, 12(4): 1512-1523. Article (CrossRef Link)
[12] Yang, Q.; He, S.; Li, J.; Chen, J.; Sun, Y., "Energy-Efficient Probabilistic Area Coverage in Wireless Sensor Networks," *Vehicular Technology, IEEE Transactions on*, vol.PP, no.99, pp.1,1, 2014. Article (CrossRef Link)
[13] Ostovari, P.; Dehghan, M.; Jie Wu, "Connected Point Coverage in Wireless Sensor Networks Using Robust Spanning Trees," in *Proc. of Distributed Computing Systems Workshops (ICDCSW), 2011 31st International Conference on* , vol., no., pp.287,293, 20-24 June 2011. Article (CrossRef Link)
[14] Shibo He; Jiming Chen; Xu Li; Shen, X.S.; Youxian Sun, "Mobility and Intruder Prior Information Improving the Barrier Coverage of Sparse Sensor Networks," *Mobile Computing, IEEE Transactions on* , vol.13, no.6, pp.1268,1282, June 2014. Article (CrossRef Link)
[15] S. Meguerdichian, S. Slijepcevic, V. Karayan, M. Potkonjak, "Localized Algorithms in Wireless Ad-hoc Networks: Location Discovery and Sensor Exposure," *Proceeding of ACM Mobihoc'01*, 106-116, Long Beach, CA, USA, 2001. Article (CrossRef Link)
[16] S. Kumar, T. Lai, and A. Arora, "Barrier coverage with wireless sensors," in *Proc. of Int. Conf.*

MobiCom, Cologne, Germany, 2005. Article (CrossRef Link)
[17] A. Chen, S. Kumar, and T. Lai, "Designing localized algorithms for barrier coverage," in *Proc. of Int. Conf. MobiCom*, Montréal, QC, Canada, 2007. Article (CrossRef Link)
[18] B. Liu, O. Dousse, J. Wang, and A. Saipulla, "Strong barrier coverage of wireless sensor networks," in *Proc. of ACM Int. Symp. MobiHoc*, Hong Kong, China, 2008. Article (CrossRef Link)
[19] A. Chen, T. Lai, and D. Xuan, "Measuring and guaranteeing quality of barrier-coverage in wireless sensor networks," in *Proc. of ACM Int. Symp. MobiHoc*, Hong Kong, China, 2008. Article (CrossRef Link)
[20] A. Saipulla, C. Westphal, B. Liu, and J. Wang, "Barrier coverage of line-based deployed wireless sensor networks," in *Proc.of IEEE Conf. INFOCOM*, Rio de Janeiro, Brazil, 2009. Article (CrossRef Link)
[21] G. Yang and D. Qiao, "Barrier information coverage with wireless sensors," in *Proc. of IEEE Conf. INFOCOM*, Rio de Janeiro, Brazil, 2009. Article (CrossRef Link)
[22] J. Li, J. Chen, and T. H. Lai, "Energy-efficient intrusion detection with a barrier of probabilistic sensors," in *Proc. of IEEE INFOCOM*, pp. 118 – 126, 2012. Article (CrossRef Link)
[23] Y. Wang and G. Cao, "On Full-View Coverage in Camera Sensor Networks," in *Proc. of IEEE INFOCOM*, 2011. Article (CrossRef Link)
[24] Y. Wang and G. Cao, "Barrier Coverage in Camera Sensor Networks," in *Proc. of ACM MobiHoc*, 2011. Article (CrossRef Link)
[25] H. Ma, M. Yang, D. Li, Y. Hong, and W. Chen, "Minimum Camera Barrier Coverage in Wireless Camera Sensor Networks," In *Proc. Of IEEE INFOCOM*, pp. 217 – 225, 2012. Article (CrossRef Link)
[26] D. Tao, S. Tang, H. Zhang, X. Mao, and H. Ma, "Strong Barrier Coverage in Directional Sensor Networks," *Computer Communications*, 35(8):895 – 905, 2012. Article (CrossRef Link)
[27] S. He, J. Chen, X. Li, X. Shen, and Y. Sun, "Cost-effective barrier coverage by mobile sensor networks," in *Proc. of IEEE INFOCOM*, pp. 819 – 827, 2012. Article (CrossRef Link)
[28] E.N. Gilbert, "Random Plane Networks," *J. SIAM*, vol. 9, no. 4, pp. 533-543, Dec. 1961. Article (CrossRef Link)
[29] M. D. Penrose, "The longest edge of the random minimal spanning tree," *Anna. Probab*., vol. 7, no. 2, pp. 340–361, 1997. Article (CrossRef Link)
[30] P. Gupta and P. R. Kumar, "Critical power for asymptotic connectivity in wireless networks," in *Proc. of Stochastic Anal., Control, Optim. Appl.*, pp. 657–566, 1998. Article (CrossRef Link)
[31] E. Bertin, J.-M. Billot, and R. Drouilhet, "Continuum Percolation in the Gabriel Graph," *Advances in Applied Probability*, vol. 34, no. 4, pp. 689-701, 2002. Article (CrossRef Link)
[32] K.R. Gabriel and R.R. Sokal, "A New Statistical Approach to Geographic Variation Analysis," *Systematic Zoology*, vol. 18, no. 3, pp. 259-278, Sept. 1969. Article (CrossRef Link)
[33] L. Booth, J. Bruck, M. Franceschetti, and R. Meester, "Covering Algorithms, Continuum Percolation and the Geometry of Wireless Networks," *Annals of Applied Probability*, vol. 13, no. 2, pp. 722-741, 2003. Article (CrossRef Link)
[34] I. Glauche, W. Krause, R. Sollacher, and M. Greiner, "Continuum Percolation of Wireless Ad Hoc Communication Networks," *Physica A*, vol. 325, pp. 577-600, 2003. Article (CrossRef Link)
[35] A. Jiang and J. Bruck, "Monotone Percolation and the Topology Control of Wireless Networks," in *Proc. of IEEE INFOCOM '05*, pp. 327-338, 2005. Article (CrossRef Link)
[36] B. Liu and D. Towsley, "A Study of the Coverage of Large-Scale Sensor Networks," in *Proc. of First IEEE Int'l Conf. Mobile Ad-Hoc and Sensor Systems (MASS '04)*, pp. 475-483, 2004. Article (CrossRef Link)
[37] Ammari, H.M.; Das, S.K., "Critical Density for Coverage and Connectivity in Three-Dimensional Wireless Sensor Networks Using Continuum Percolation," *Parallel and Distributed Systems, IEEE Transactions on* , vol.20, no.6, pp.872,885, June 2009. Article (CrossRef Link)
[38] Khanjary, M.; Sabaei, M.; Meybodi, M.R., "Critical Density for Coverage and Connectivity in Two-Dimensional Aligned-Orientation Directional Sensor Networks Using Continuum Percolation," *Sensors Journal, IEEE*, vol.14, no.8, pp.2856,2863, Aug. 2014.

Article (CrossRef Link)
[39] R. Meester and R. Roy, "Continuum Percolation," Cambridge, U.K.: Cambridge University Press, 1996. Article (CrossRef Link)
[40] H. Ma and Y. Liu, "Some problems of directional sensor networks," *Int. J. Sensor Netw.*, vol. 2, no. 2, pp. 44–52, 2007. Article (CrossRef Link)
[41] E. Hörster and R. Lienhart, "Approximating optimal visual sensor placement," in *Proc. of IEEE Int. Conf. Multimedia Expo*, Jul. 2006, pp. 1257–1260. Article (CrossRef Link)
[42] S. Ram, K. R. Ramakrishnan, P. K. Atrey, V. K. Singh, and M. S. Kankanhalli, "A design methodology for selection and placement of sensors in multimedia surveillance systems," in *Proc. of 4th ACM Int. Workshop Video Surveill. Sensor Netw.*, 2006, pp. 121–130.
Article (CrossRef Link)

Xiaoshuang Liu received the M.S. degree from Hebei Normal University, Hebei, China, in 2012. She is currently working toward the Ph.D. degree in communication and information system at the School of Information and Communication Engineering, Beijing University of Posts and Telecommunications, Beijing, China. Her research interests include optimization, wireless sensor network, et al.

Guixia Kang received the M.S. degree from Tianjin University, Tianjin, China, and the Ph.D. degree in electrical engineering from Beijing University of Posts and Telecommunications (BUPT), Beijing. She was a research scientist in the Future Radio Concept Department of Siemens, Munich, Germany. She is currently a Professor with BUPT. Her interests include the research, development and standardization of 3G and beyond 3G (B3G) wireless communications systems as well as wireless sensor networks.

Ningbo Zhang received his Ph. D. degree from the Beijing University of Posts andTeleco mmunications, China in 2010. After that, he worked in the Huawei Technology as a senior r esearcher. From 2010 to 2014, he worked for 3GPP and proposed more than 100 contributio ns. From 2014 to now, he worked in the Beijing University of Posts and Telecommunicatios . His research interests include M2M communication, D2D communication, advanced channel coding and modulation, cooperative communication and cognitive radio etc.